Nano Research
2023, 16(2): 2059–2064

ISSN 1998-0124 CN 11-5974/O4
https://doi.org/10.1007/s12274-022-4878-3

Research Article

Low-loading gold *in situ* doped with sulfur by biomolecule-assisted approach for promoted electrochemical carbon dioxide reduction

Meijie Tan[1,§], Xiaoqian Han[1,§], Sen Ru[2], Chao Zhang[1], Zhouru Ji[1], Zhaolin Shi[1], Guomeng Qiao[1], Yunying Wang[1], Ruixue Cui[1], Qiquan Luo[2] (✉), Jiqing Jiao[1,3,4] (✉), Yaguang Li[5], and Tongbu Lu[1,3]

[1] *MOE International Joint Laboratory of Materials Microstructure, Institute for New Energy Materials and Low Carbon Technologies, School of Materials Science and Engineering, Tianjin University of Technology, Tianjin 300384, China*
[2] *Institutes of Physical Science and Information Technology, Anhui University, Hefei 230601, China*
[3] *Haihe Laboratory of Sustainable Chemical Transformations, Tianjin 300192, China*
[4] *College of Materials Science and Engineering, State Key Laboratory of Bio-Fibers and Eco-Textiles, Qingdao University, Qingdao 266071, China*
[5] *Hebei Key Lab of Optic-electronic Information and Materials, College of Physics Science and Technology, Institute of Life Science and Green Development, Hebei University, Baoding 071002, China*
[§] *Meijie Tan and Xiaoqian Han contributed equally to this work.*

Received: 1 July 2022 / **Revised:** 5 August 2022 / **Accepted:** 7 August 2022

ABSTRACT

For electrochemical carbon dioxide reduction (CO_2RR), CO_2-to-CO conversion is considered an ideal route towards carbon neutrality for practical applications. Gold (Au) is known as a promising catalyst with high selectivity for CO; however, it suffers from high cost and low mass-specific activity. In this study, we design and prepare a catalyst featuring uniform S-doped Au nanoparticles on N-doped carbon support (denoted as S-Au/NC) by an *in situ* synthesis strategy using biomolecules. The S-Au/NC displays high activity and selectivity for CO in CO_2RR with a Au loading as low as 0.4 wt.%. The Faradaic efficiency of CO (FE_{CO}) for S-Au/NC is above 95% at −0.75 V (vs. RHE); by contrast, the FE_{CO} of Au/NC (without S) is only 58%. The Tafel slope is 77.4 mV·dec^{-1}, revealing a favorable kinetics process. Furthermore, S-Au/NC exhibits an excellent long-term stability for CO_2RR. Density functional theory (DFT) calculations reveal that the S dopant can boost the activity by reducing the free energy change of the potential-limiting step (formation of the *COOH intermediate). This work not only demonstrates a model catalyst featuring significantly reduced use of noble metals, but also establishes an *in situ* synthesis strategy for preparing high-performance catalysts.

KEYWORDS

electrochemical CO_2 reduction, nanocomposites, heterogeneous catalyst, *in situ* sulfured, heteroatoms

1 Introduction

Global warming is a critical issue facing humankind, which demands scientists to explore renewable energy sources and decrease carbon dioxide (CO_2) emission. Electrochemical CO_2 reduction (CO_2RR) can be operated under ambient temperature and pressure, and thus offers an ideal route towards carbon neutrality by converting renewable electricity into carbon-containing chemical feedstocks. Among the different CO_2RR products (CO, HCOOH, C_2H_4, etc.), CO could be used as a feedstock for bulk chemical manufacturing. The conversion of CO_2 into CO is considered one of the most promising candidate reactions because of its high technological and economical feasibility. To achieve high-efficiency CO_2-to-CO conversion, many advanced catalysts have been developed, including single-atomic site catalysts [1–6], molecular catalysts [4–7], alloys [8–9], and metal-free carbon-based catalysts [10–12]. Among these advanced catalysts, gold (Au) is known as a promising catalyst that exhibits high catalytic activity and high selectivity for CO [13–16]. However, Au is of high cost, and also susceptible to poisoning, which constrains its large-scale applications.

Tremendous research efforts have been made to improve the electrocatalytic performance of Au for CO_2RR, aiming at reducing the use and improving the mass-specific activity of Au. The specific surface area would be vastly increased when the material is downsized to nanoscale. Sun et al. reported that monodisperse Au nanoparticles 8 nm in size showed the maximum Faradaic efficiency for CO (FE_{CO}) of 90% at −0.67 V (vs. RHE) [17]. The surface structures of catalysts, such as faces, corners, and edges, play critical roles in heterogeneous catalysis [13]. It has been reported that for Au nanoparticles, the edge sites are more selective for CO, whereas the corner sites prefer to give H_2 [18]. Different morphologies for Au nanoparticles, such as nanowires [15], nanoneedles [19], and nanoporous Au [20], have been reported, demonstrating high selective CO_2 reduction to CO for CO_2RR. In addition, for pure Au catalyst, theoretical simulations suggested that the *COOH formation step has the largest free energy change, and this potential-limiting step (PLS) hinders the activity and selectivity for CO for CO_2RR [19, 21, 22]. Introducing heteroatoms [23, 24] could alter the electronic structure of Au, and thus is an effective strategy to reduce the free

Address correspondence to Qiquan Luo, qluo@ahu.edu.cn; Jiqing Jiao, jiaojiqing101@163.com

energy change for the PLS [25]. Kanan et al. prepared oxide-derived Au featuring metastable surfaces, which exhibited highly FE_{CO} at low overpotentials [26]. Compared with O (oxygen) and N (nitrogen), S (sulfur) can enhance the local electron density around the active sites because of its lower electronegativity [27, 28], and thus may promote the proton-coupled electron transfer to key intermediates [29, 30]. However, the studies on S dopant in Au-based catalysts for CO_2RR are still rather scarce.

In this work, we designed and prepared the catalyst featuring S-modified uniform Au nanoparticles on N-doped carbon support (denoted as S-Au/NC) by *in situ* synthesis strategy using biomolecule. The adsorbed L-cysteine (Cys) of Au_{25} offers the S source and metal–organic frameworks (MOF) was conversed into N-doped carbon matrix. The S-Au/NC displayed high activity and selectivity for CO in CO_2RR with a Au loading as low as 0.4 wt.%. The FE_{CO} for S-Au/NC is above 95% at −0.75 V (vs. RHE); by contrast, the FE_{CO} of Au/NC (without S) is only 58%. The Tafel slope is 77.4 mV·dec^{-1}, revealing a favorable kinetics for CO generation. Density functional theory (DFT) calculations revealed that S-doped would help to reduce the free energy change of the PLS (that is, formation of the *COOH intermediate). This work not only demonstrates a model catalyst featuring significantly reduced use of noble metals, but also establishes an *in situ* synthesis strategy for preparing high-performance catalysts.

2 Experimental

Synthesis of *in situ* S-doped Au nanoparticles: in a typical procedure, $Zn(NO_3)_2{\cdot}5H_2O$ (0.74 g) and 2-methylimidazole (1.64 g) were dissolved separately into methanol (25 mL), and then the solution of 2-methylimidazole was subsequently poured into the solution of $Zn(NO_3)_2{\cdot}6H_2O$. After mixing and stirring at room temperature for 24 h, the solid (ZIF-8) was centrifuged and washed with methanol three times. The prepared ZIF-8 was ultrasonically dispersed into methanol (20 mL). And Au_{25}-Cys aqueous solution (100 mL) was dropwisely added into the ZIF-8 solution and stirred for 3 h. It was centrifuged and washed with water and ethanol for three times. Subsequently, the solid was dried in vacuum at 60 °C for 6 h. Finally, the sample was placed in a tube furnace and heated to 1,000 °C for 1 h with a ramping rate of 5 °C·min^{-1} under Ar to yield S-Au/NC.

The synthesis of Au_{25}-Cys, NC, Au_{25}-Cys/NC, and Au/NC composites can be found in Electronic Supplementary Material (ESM). The electrochemical measurements, characterizations, and computational methods were illustrated in the ESM.

3 Results and discussion

Figure 1(a) illustrates the *in situ* synthesis strategy for the S-Au nanoparticles on N-doped carbon matrix. First, Au_{25} clusters capped with Cys biomolecules (denoted as Au_{25}-Cys) were synthesized according to previous reports [31, 32]. Subsequently, the composite comprising Au_{25}-Cys clusters and ZIF-8 particles was subjected to pyrolysis, during which S-doped Au nanoparticles were *in situ* formed. By adjusting the loading amount of Au_{25}-Cys clusters, Au nanoparticles with uniform sizes could form on the N-doped carbon support. As shown in the transmission electron microscopy (TEM) image (Fig. 1(b)), ZIF-8 particles are around 100 nm in size. The Au_{25}-Cys clusters were mixed with ZIF-8 in ethanol under ultrasonication, and the

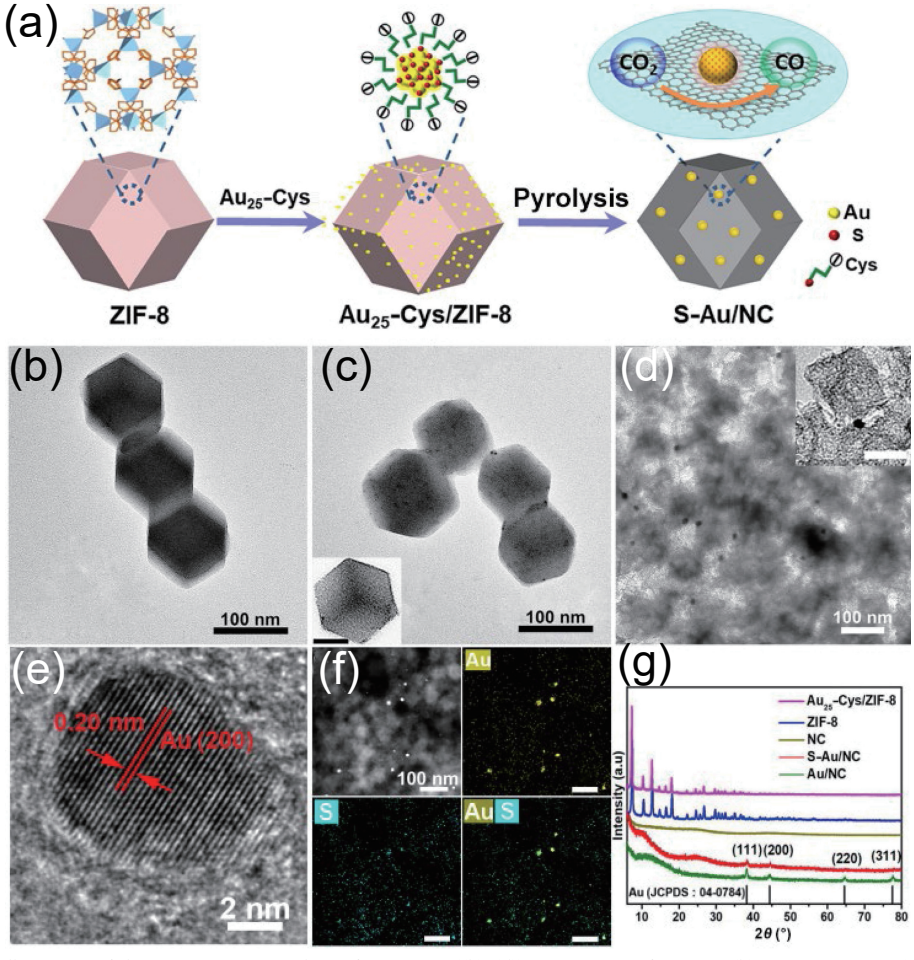

Figure 1 (a) Schematic illustration of the preparation procedure of S-Au/NC. ((b)–(d)) TEM images for ZIF-8 (b), Au_{25}-Cys/ZIF-8 (c), and S-Au/NC (d). (e) HRTEM image of S-doped Au. (f) EDS mapping results for Au and S. (g) XRD patterns for ZIF-8, Au_{25}-Cys/ZIF-8, Au/NC, and S-Au/NC.

clusters were evenly adsorbed onto the surface of ZIF-8 (Fig. 1(c) and Fig. S1 in the ESM). After pyrolysis at 1,000 °C for 1 h, the small Au_{25}-Cys clusters disappeared (Fig. 1(d)), and larger Au nanoparticles (~ 10 nm in size) were found on the carbon support. The high-resolution TEM (HRTEM) image (Fig. 1(e)) of the Au nanoparticles shows clear lattice fringes with a spacing of 0.21 nm, which corresponds to the (200) facets of face-center cubic phase Au. The TEM images for Au/NC could be seen in Fig. S3 in the ESM. The Au loading of S-Au/NC was determined to be 0.4 wt.% via inductively coupled plasma optical emission spectroscopy (ICP-OES), whereas Au loading of Au/NC is 10 wt.% (Table S1 in the ESM). The elemental distribution of Au and S was confirmed by energy-dispersive X-ray spectroscopy (EDS) elemental mapping (Fig. 1(f)). It is noticeable that the signals of S overlap well with the signals of Au. The EDS mapping results for C and N are shown in Fig. S2 in the ESM. The XRD pattern (Fig. 1(g)) shows the diffraction peaks (111), (200), (220), and (311) characteristic of face-centered cubic Au (JCPDS No. 04-0784); notably, no diffraction peaks characteristic of Au_xS were found in S-Au/NC catalyst, suggesting that the S atoms are doped in Au nanoparticles by *in situ* synthesis.

Figure 2(a) shows the UV–visible absorption spectrum of the prepared Au_{25}-Cys clusters. The four characteristic peaks located at 440, 545, 670, and 780 nm can be clearly identified, indicating that the Au_{25}-Cys clusters were successfully obtained. As the –SH group in Cys has a strong affinity to Au, the Cys biomolecules are adsorbed on the surface of Au_{25}. This process was validated by the Fourier transform infrared spectroscopy (FTIR). Figure 2(b) shows the FTIR spectra of Cys, Au_{25}-Cys, Au_{25}-Cys/ZIF-8, and S-Au/NC. For Cys, the bands located around 1,590 and 1,390 cm^{-1} corresponds to the asymmetric and symmetric stretching of COO^-; the bands in the range of 3,000–3,500 and 1,542 cm^{-1} can be assigned to the $-NH_3^+$ stretching and N–H bending vibrations, respectively. Besides, the weak band at 2,556 cm^{-1} confirmed the presence of the –SH group [33]. By contrast, in the spectral profiles for Au_{25}-Cys and Au_{25}-Cys/ZIF-8, the band typical of –SH group disappeared, which confirmed the formation of Au–S bonds on the surface of Au clusters. The adsorbed Cys biomolecules on the surface of Au_{25} could serve as the S source for following reactions. After pyrolysis, the S-Au/NC catalyst was obtained via the biomolecule-assisted synthesis approach. The chemical composition and structure were examined by X-ray photoelectron spectroscopy (XPS) (Fig. S4 in the ESM) [34]. As shown in Fig. 2(c), the high-resolution XPS profile of S 2p can be deconvoluted into four peaks. The peaks at 164.1 and 165.2 eV represent S $2p_{3/2}$ and S $2p_{1/2}$ in the form of –C–S–C– in carbon sp^2 structure [30, 35]; the two peaks at 162.3 and 163.1 eV can be ascribed to S $2p_{3/2}$ and S $2p_{1/2}$ for S-doped Au [36]. On the basis of the above analysis, the S-doped Au/NC was synthesized successfully via *in situ* sulfidation using biomolecule.

The electrocatalytic performance for CO_2RR was assessed in 0.1 M $KHCO_3$ electrolyte in an H-type cell. The electroreduction activity was first evaluated via linear sweep voltammetry (LSV). The prepared Au/NC, Au_{25}-Cys/NC, and NC were used as reference samples. The S-Au/NC displayed the highest total current density and the lowest onset potential (Fig. 3(a) inset). The higher current density over S-Au/NC than over Au_{25}-Cys/NC, S-Au/NC reveals that the effect of S doping is more efficient than that of –SH adsorption. In particular, the catalytic activity of S-Au/NC was significantly higher than that of Au/NC, indicating that the S doping for Au would help to improve activity for CO_2RR. Potentiostatic electrolysis was conducted to evaluate the FE_{CO}. H_2 and CO are the only products identified by gas chromatography (GC) analysis (Fig. S5 in the ESM) and ^1H NMR spectroscopy (Fig. S6 in the ESM). As Fig. 3(b) clearly shows, the

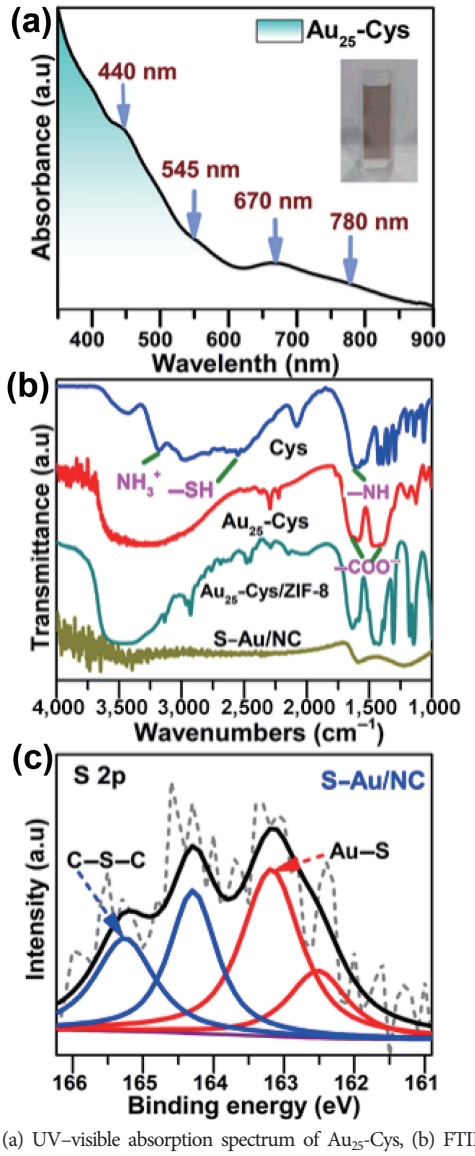

Figure 2 (a) UV–visible absorption spectrum of Au_{25}-Cys, (b) FTIR spectra for Cys, Au_{25}-Cys, Au_{25}-Cys/ZIF-8, and S-Au/NC. (c) The high-resolution XPS profile of S 2p.

FE_{CO} value of S-Au/NC is greater than 85% over a wide potential range from −0.55 to −0.85 V (vs. RHE), and reaches the maximum value of 95% at −0.75 V (vs. RHE). By contrast, the Au/NC and Au_{25}-Cys/NC achieve maximum FE_{CO} values (58% and 62%, respectively) at −0.75 V (vs. RHE). The CO partial current density (j_{CO}) of S-Au/NC is also significantly higher, achieving 15.2 mA·cm^{-2} at −0.75 V (vs. RHE), which is approximately 5.0, 3.3, and 5.2 times larger than those of Au/NC, Au_{25}-Cys/NC, and NC, respectively (Fig. 3(c)). The Au/NC was prepared with the same loading with S-Au/NC (0.4 wt.%). As shown in Fig. S7 in the ESM, it displays the low total current density and low FE_{CO}. The FE_{CO} is only 62% at −0.75 V (vs. RHE), which is lower than those of S-Au/NC. By introducing S atoms into Au, the activity and FE_{CO} of the S-Au/NC was significantly improved over the entire range of tested potentials.

The Tafel plot regarding j_{CO} reveals the reaction kinetics of different catalysts (Fig. 3(d)). The Tafel slope for S-Au/NC is 77.4 mV·dec^{-1}, which is the smallest value among those prepared catalysts. By contrast, the Tafel slopes of Au/NC, Au_{25}-Cys/NC, and NC are 179.5, 175.7, and 244.7 mV·dec^{-1}, respectively. It reveals that the step of electron and proton transfer (formation of the *COOH intermediate) is the PLS for CO_2RR [39]. The S-doped Au shows a favorable kinetics for CO formation during

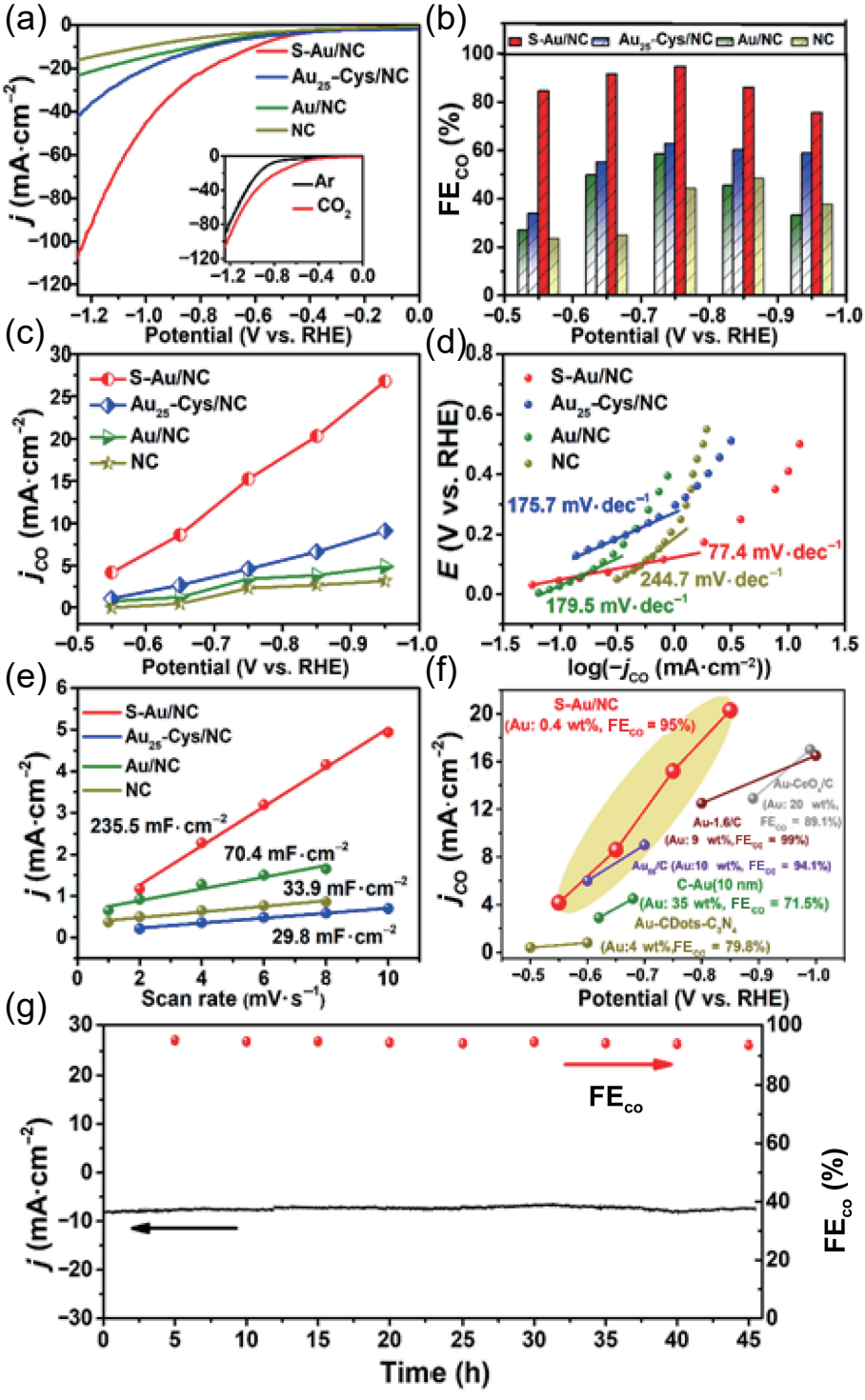

Figure 3 (a) LSV, (b) FE_{CO}, (c) j_{CO}, (d) Tafel plots, (e) plots of the current density versus the scan rate for S-Au/NC (0.4 wt.%), Au/NC (10 wt.%), Au_{25}-Cys/NC, and NC in CO_2-saturated in 0.1 M $KHCO_3$ solution. (f) Comparison of j_{CO} and FE_{CO} (maxima) for state-of-the-art Au catalysts (Au-CDots-C_3N_4 [37], C-Au [17], Au_{55}-C [38], Au-1.6-C [14], and Au-CeO_x/C [16]) with high loadings. (g) Long-term operation test and the corresponding FE_{CO} of S-Au/NC at −0.75 V (vs. RHE).

CO_2RR. From the N_2 adsorption–desorption isotherm, it can be seen that the Brunauer–Emmett–Teller (BET) surface area of S-Au/NC (1,123.4 $m^2 \cdot g^{-1}$) was larger than that of NC (775.4 $m^2 \cdot g^{-1}$) (Fig. S8 in the ESM). To reveal the intrinsic activity, the double layer capacitance (C_{dl}) was determined via cyclic voltammetry (CV) (Fig. S9 in the ESM). As shown in Fig. 3(e), the C_{dl} for S-Au/NC (235.5 $mF \cdot cm^{-2}$) was much higher than those of the other samples (70.4 $mF \cdot cm^{-2}$ for Au/NC, 29.8 $mF \cdot cm^{-2}$ for Au_{25}-Cys/NC, and 33.9 $mF \cdot cm^{-2}$ for NC), indicating that the S-Au/NC has a larger electrochemical active surface area than the others. In particular, as shown in Fig. 2(f), compared with those of other state-of-the-art Au catalysts with high loadings, the high FE_{CO} and j_{CO} can be obtained by using S-Au/NC with a low loading (0.4 wt.%). Notably, the content of Au of S-Au/C is the smallest among recently reported data. Furthermore, S-Au/NC exhibited an excellent long-term stability for CO_2RR; the current density showed no significant decay and the FE_{CO} maintained at > 92% after 45 h continuous electrolysis (Fig. 3(g)).

We carried out DFT calculations to unveil the underpinning mechanism of CO_2RR on the catalysts [40–43]. The structural model for Au(100) is shown in Fig. 4. The model with one surface Au atom of the Au(100) surface replaced by a S atom was constructed to mimic the S-doped Au catalyst (denoted as S-Au(100)). In order to successfully obtain the most stable structures

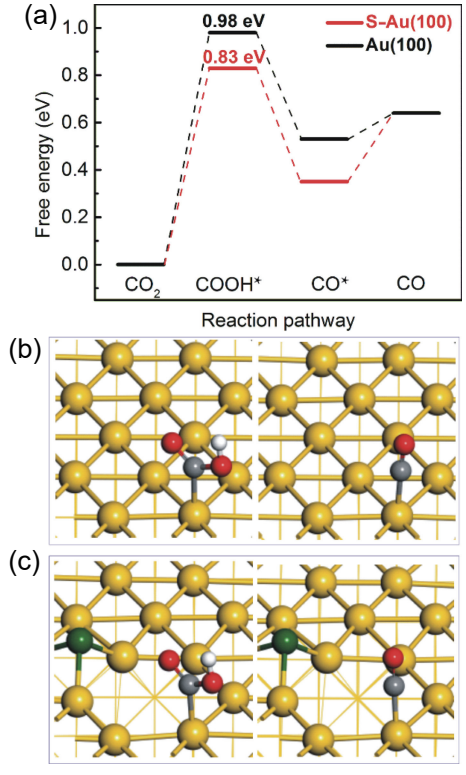

Figure 4 (a) Gibbs free energy diagrams for the CO_2RR on Au(100) (black line) and S-Au(001) (red line) at zero potential. The optimized adsorption configurations for the various intermediates on Au(100) (b) and S-Au(100) (c). Au atom in gold, S atom in green, C atom in gray, O atom in red, and H atom in white, respectively.

of S-Au(100), we conducted *ab initio* molecular dynamics simulations (AIMD) (Fig. S10 in the ESM). Several local-minimal-energy structures were selected for further structural optimization firstly, and then the most stable configuration was used for further calculations. We next calculated the free energy diagram for CO_2RR to CO on the Au(100) (in black line) and S-Au(100) (in red line) surface. As shown in Fig. 4(a), the formation of the *COOH intermediate was found to be the PLS for both models. The calculated free energy changes are 0.98 and 0.83 eV for Au(100) and S-Au(100), respectively (Table S2 in the ESM). The most stable configurations of *COOH and *CO adsorption on Au(100) and S-Au(100) were shown in Figs. 4(b) and 4(c), respectively. To unveil the origin of the stronger adsorption for the key intermediate COOH on S-Au(100) than on Au(100), the d-band centers of the two models were computed (Fig. S11 in the ESM). S-Au(100) has a value of −3.16 eV (slightly closer to its Fermi level), and this in turns leads to the strengthened adsorption. These results clearly show that by rationally introducing S dopants into Au catalysts, the structure of catalytic sites could be tuned and the CO_2RR performance could be boosted accordingly. The theoretical calculation results are in good agreement with the experimental data.

4 Conclusions

For CO_2RR, reducing the use of Au and improving its mass-specific activity are considered as promising strategies for practical applications. In this work, we designed and prepared the catalyst featuring uniform S-Au/NC by *in situ* synthesis strategy using biomolecules. The Au_{25}-Cys clusters were synthesized first, and the adsorbed Cys on Au_{25} served as the S source. The MOF was converted into N-doped carbon matrix after pyrolysis. The S-Au/NC displayed high activity and selectivity for CO in CO_2RR with a Au loading as low as 0.4 wt.%. The FE_{CO} value of S-Au/NC is greater than 85% over a wide potential range from −0.55 to −0.85 V (vs. RHE), and reaches the maximum value of 95% at −0.75 V (vs. RHE). By contrast, the Au/NC and Au_{25}-Cys/NC achieve maximum FE_{CO} values respectively of 58% and 62%, at the same potential. The Tafel slope of S-Au/NC is 77.4 mV·dec^{-1}, implying a favorable kinetics for CO generation. Furthermore, after 45 h continuous electrolysis, the current density showed no significant decline and the FE_{CO} was maintained at > 92%, revealing an excellent stability. DFT and AIMD calculations show that the S dopants would help to reduce the free energy change for the PLS, which improved the activity for CO_2RR. This work demonstrates a model catalyst featuring significantly reduced use of noble metals, and offers a promising approach for CO_2RR practical applications.

Acknowledgements

The work was financially supported by the National Natural Science Foundation of China (Nos. 52072260, 21931007, 21790052, and U21A20317), the Science and Technology Support Program for Youth Innovation in Universities of Shangdong Province (No. 2020KJA012), the Tianjin Natural Science Foundation (Nos. 21JCZXJC00130 and B2021201074), the Haihe Laboratory of Sustainable Chemical Transformations, National Key R&D Program of China (No. 2017YFA0700104), and the University Synergy Innovation Program of Anhui Province (No. GXXT-2020-001). Supercomputing of Anhui University and National Supercomputing Center in Shanghai was acknowledged for computational support.

Electronic Supplementary Material: Supplementary material (experimental section, computational methods, supplementary figures, and supplementary table) is available in the online version of this article at https://doi.org/10.1007/s12274-022-4878-3.

References

[1] Lin, L.; Li, H. B.; Wang, Y.; Li, H. F.; Wei, P. F.; Nan, B.; Si, R.; Wang, G. X.; Bao, X. H. Temperature-dependent CO_2 electroreduction over Fe–N–C and Ni–N–C single-atom catalysts. *Angew. Chem. Int. Ed.* **2021**, *60*, 26582–26586.

[2] Li, R. Z.; Wang, D. S. Understanding the structure-performance relationship of active sites at atomic scale. *Nano Res.* **2022**, *15*, 6888–6923.

[3] Rong, X.; Wang, H. J.; Lu, X. L.; Si, R.; Lu, T. B. Controlled synthesis of a vacancy-defect single-atom catalyst for boosting CO_2 electroreduction. *Angew. Chem. Int. Ed.* **2020**, *59*, 1961–1965.

[4] Zheng, X. B.; Li, B. B.; Wang, Q. S.; Wang, D. S.; Li, Y. D. Emerging low-nuclearity supported metal catalysts with atomic level precision for efficient heterogeneous catalysis. *Nano Res.* **2022**, *15*, 7806–7839.

[5] Zhu, P.; Xiong, X.; Wang, D. S. Regulations of active moiety in single atom catalysts for electrochemical hydrogen evolution reaction. *Nano Res.* **2022**, *15*, 5792–5815.

[6] Zheng, X. B.; Yang, J. R.; Xu, Z. F.; Wang, Q. S.; Wu, J. B.; Zhang, E. H.; Dou, S. X.; Sun, W. P.; Wang, D. S.; Li, Y. D. Ru–Co pair sites catalyst boosts the energetics for the oxygen evolution reaction. *Angew. Chem. Int. Ed.* **2022**, *134*, e202205946.

[7] Jin, S.; Hao, Z. M.; Zhang, K.; Yan, Z. H.; Chen, J. Advances and challenges for the electrochemical reduction of CO_2 to CO: From fundamentals to industrialization. *Angew. Chem. Int. Ed.* **2021**, *60*, 20627–20648.

[8] Jiao, J. Q.; Zhang, N. N.; Zhang, C.; Sun, N.; Pan, Y.; Chen, C.; Li, J.; Tan, M. J.; Cui, R. X.; Shi, Z. L. et al. Doping ruthenium into metal matrix for promoted pH-universal hydrogen evolution. *Adv. Sci.* **2022**, *9*, 2200010.

[9] Yun, Y. P.; Sheng, H. T.; Bao, K.; Xu, L.; Zhang, Y.; Astruc, D.; Zhu, M. Z. Design and remarkable efficiency of the robust sandwich

cluster composite nanocatalysts ZIF-8@Au_{25}@ZIF-67. *J. Am. Chem. Soc.* **2020**, *142*, 4126–4130.

[10] Wu, J. J.; Yadav, R. M.; Liu, M. J.; Sharma, P. P.; Tiwary, C. S.; Ma, L. L.; Zou, X. L.; Zhou, X. D.; Yakobson, B. I.; Lou, J. et al. Achieving highly efficient, selective, and stable CO_2 reduction on nitrogen-doped carbon nanotubes. *ACS Nano* **2015**, *9*, 5364–5371.

[11] Wang, Y. F.; Li, Y. X.; Wang, Z. Y.; Allan, P.; Zhang, F. C.; Lu, Z. G. Reticular chemistry in electrochemical carbon dioxide reduction. *Sci. China Mater.* **2020**, *63*, 1113–1141.

[12] Li, Z.; Ji, S. F.; Liu, Y. W.; Cao, X.; Tian, S. B.; Chen, Y. J.; Niu, Z. Q.; Li, Y. D. Well-defined materials for heterogeneous catalysis: From nanoparticles to isolated single-atom sites. *Chem. Rev.* **2020**, *120*, 623–682.

[13] Zhao, S.; Jin, R. X.; Jin, R. C. Opportunities and challenges in CO_2 reduction by gold- and silver-based electrocatalysts: From bulk metals to nanoparticles and atomically precise nanoclusters. *ACS Energy Lett.* **2018**, *3*, 452–462.

[14] Souza, M. L.; Lima, F. H. B. Dibenzyldithiocarbamate-functionalized small gold nanoparticles as selective catalysts for the electrochemical reduction of CO_2 to CO. *ACS Catal.* **2021**, *11*, 12208–12219.

[15] Zhu, W. L.; Zhang, Y. J.; Zhang, H. Y.; Lv, H. F.; Li, Q.; Michalsky, R.; Peterson, A. A.; Sun, S. H. Active and selective conversion of CO_2 to CO on ultrathin Au nanowires. *J. Am. Chem. Soc.* **2014**, *136*, 16132–16135.

[16] Gao, D. F.; Zhang, Y.; Zhou, Z. W.; Cai, F.; Zhao, X. F.; Huang, W. G.; Li, Y. S.; Zhu, J. F.; Liu, P.; Yang, F. et al. Enhancing CO_2 electroreduction with the metal-oxide interface. *J. Am. Chem. Soc.* **2017**, *139*, 5652–5655.

[17] Zhu, W. L.; Michalsky, R.; Metin, Ö.; Lv, H. F.; Guo, S. J.; Wright, C. J.; Sun, X. L.; Peterson, A. A.; Sun, S. H. Monodisperse Au nanoparticles for selective electrocatalytic reduction of CO_2 to CO. *J. Am. Chem. Soc.* **2013**, *135*, 16833–16836.

[18] Mistry, H.; Reske, R.; Zeng, Z. H.; Zhao, Z. J.; Greeley, J.; Strasser, P.; Cuenya, B. R. Exceptional size-dependent activity enhancement in the electroreduction of CO_2 over Au nanoparticles. *J. Am. Chem. Soc.* **2014**, *136*, 16473–16476.

[19] Guo, H.; Si, D. H.; Zhu, H. J.; Li, Q. X.; Huang, Y. B.; Cao, R. Ni single-atom sites supported on carbon aerogel for highly efficient electroreduction of carbon dioxide with industrial current densities. *eScience* **2022**, *2*, 295–303.

[20] Hossain, M. N.; Liu, Z. G.; Wen, J. L.; Chen, A. C. Enhanced catalytic activity of nanoporous Au for the efficient electrochemical reduction of carbon dioxide. *Appl. Catal. B: Environ.* **2018**, *236*, 483–489.

[21] Back, S.; Yeom, M. S.; Jung, Y. Active sites of Au and Ag nanoparticle catalysts for CO_2 electroreduction to CO. *ACS Catal.* **2015**, *5*, 5089–5096.

[22] Cao, T.; Lin, R.; Liu, S. J.; Cheong, W. C.; Li, Z.; Wu, K. L.; Zhu, Y. Q.; Wang, X. L.; Zhang, J.; Li, Q. H. et al. Atomically dispersed Ni anchored on polymer-derived mesh-like N-doped carbon nanofibers as an efficient CO_2 electrocatalytic reduction catalyst. *Nano Res.* **2022**, *15*, 3959–3963.

[23] Jiao, J. Q.; Yang, W. J.; Pan, Y.; Zhang, C.; Liu, S. J.; Chen, C.; Wang, D. S. Interface engineering of partially phosphidated Co@Co-P@NPCNTs for highly enhanced electrochemical overall water splitting. *Small* **2020**, *16*, 2002124.

[24] Wang, Y.; Zheng, X. B.; Wang, D. S. Design concept for electrocatalysts. *Nano Res.* **2022**, *15*, 1730–1752.

[25] Li, S. T.; Nagarajan, A. V.; Alfonso, D. R.; Sun, M. K.; Kauffman, D. R.; Mpourmpakis, G.; Jin, R. C. Boosting CO_2 electrochemical reduction with atomically precise surface modification on gold nanoclusters. *Angew. Chem. Int. Ed.* **2021**, *60*, 6351–6356.

[26] Chen, Y. H.; Li, C. W.; Kanan, M. W. Aqueous CO_2 reduction at very low overpotential on oxide-derived Au nanoparticles. *J. Am. Chem. Soc.* **2012**, *134*, 19969–19972.

[27] Jia, C.; Tan, X.; Zhao, Y.; Ren, W. H.; Li, Y. B.; Su, Z.; Smith, S. C.; Zhao, C. Sulfur-dopants promoted electroreduction of CO_2 over coordinatively unsaturated Ni-N_2 moieties. *Angew. Chem. Int. Ed.* **2021**, *60*, 23342–23348.

[28] Li, M. F.; Zhang, B.; Cheng, T.; Yu, S.; Louisia, S.; Chen, C. B.; Chen, S. P.; Cestellos-Blanco, S.; Goddard, W. A.; Yang, P. D. Sulfur-doped graphene anchoring of ultrafine Au_{25} nanoclusters for electrocatalysis. *Nano Res.* **2021**, *14*, 3509–3513.

[29] Chen, S. H.; Li, W. H.; Jiang, W. J.; Yang, J. R.; Zhu, J. X.; Wang, L. Q.; Ou, H. H.; Zhuang, Z. C.; Chen, M. Z.; Sun, X. H. et al. MOF encapsulating N-heterocyclic carbene-ligated copper single-atom site catalyst towards efficient methane electrosynthesis. *Angew. Chem. Int. Ed.* **2022**, *61*, e202114450.

[30] Chen, Z. W.; Zhang, J. W.; Zhang, C.; Cui, R. X.; Tan, M. J.; Guo, S.; Wang, H. J.; Jiao, J. Q.; Lu, T. B. Regulating the coordination metal center in immobilized molecular complexes as single-atomic electrocatalysts for highly active, selective and durable electrochemical CO_2 reduction. *J. Power. Sources* **2022**, *519*, 230788.

[31] Tan, Y.; Yan, L.; Huang, C. Q.; Zhang, W. N.; Qi, H. F.; Kang, L. L.; Pan, X. L.; Zhong, Y. J.; Hu, Y.; Ding, Y. J. Fabrication of an Au_{25}-Cys-Mo electrocatalyst for efficient nitrogen reduction to ammonia under ambient conditions. *Small* **2021**, *17*, 2100372.

[32] Zhang, N. Q.; Ye, C. L.; Yan, H.; Li, L. C.; He, H.; Wang, D. S.; Li, Y. D. Single-atom site catalysts for environmental catalysis. *Nano Res.* **2020**, *13*, 3165–3182.

[33] Tai, H. L.; Nishikawa, K.; Higuchi, Y.; Mao, Z. W.; Hirota, S. Cysteine SH and glutamate COOH contributions to Ni-Fe hydrogenase proton transfer revealed by highly sensitive FTIR spectroscopy. *Angew. Chem. Int. Ed.* **2019**, *58*, 13285–13290.

[34] Bao, L. R.; Zhu, S. H.; Chen, Y.; Wang, Y.; Meng, W. H.; Xu, S.; Lin, Z. H.; Li, X. Y.; Sun, M.; Guo, L. M. Anionic defects engineering of Co_3O_4 catalyst for toluene oxidation. *Fuel* **2022**, *314*, 122774.

[35] Shi, Q. Q.; Peng, F.; Liao, S. X.; Wang, H. J.; Yu, H.; Liu, Z. W.; Zhang, B. S.; Su, D. S. Sulfur and nitrogen co-doped carbon nanotubes for enhancing electrochemical oxygen reduction activity in acidic and alkaline media. *J. Mater. Chem. A* **2013**, *1*, 14853–14857.

[36] Gadgil, B.; Damlin, P.; Viinikanoja, A.; Heinonen, M.; Kvarnström, C. One-pot synthesis of an Au/Au_2S viologen hybrid nanocomposite for efficient catalytic applications. *J. Mater. Chem. A* **2015**, *3*, 9731–9737.

[37] Zhao, S. Q.; Tang, Z. Y.; Guo, S. J.; Han, M. M.; Zhu, C.; Zhou, Y. J.; Bai, L.; Gao, J.; Huang, H.; Li, Y. Y. et al. Enhanced activity for CO_2 electroreduction on a highly active and stable ternary Au-CDots-C_3N_4 electrocatalyst. *ACS Catal.* **2018**, *8*, 188–197.

[38] Wan, X. K.; Wang, J. Q.; Wang, Q. M. Ligand-protected Au_{55} with a novel structure and remarkable CO_2 electroreduction performance. *Angew. Chem. Int. Ed.* **2021**, *133*, 20916–20921.

[39] Sun, X. H.; Tuo, Y. X.; Ye, C. L.; Chen, C.; Lu, Q.; Li, G. N.; Jiang, P.; Chen, S. H.; Zhu, P.; Ma, M. et al. Phosphorus induced electron localization of single iron sites for boosted CO_2 electroreduction reaction. *Angew. Chem. Int. Ed.* **2021**, *60*, 23614–23618.

[40] Jing, H. Y.; Zhu, P.; Zheng, X. B.; Zhang, Z. D.; Wang, D. S.; Li, Y. D. Theory-oriented screening and discovery of advanced energy transformation materials in electrocatalysis. *Adv. Powder Mater.* **2022**, *1*, 100013.

[41] Wang, B. Q.; Chen, S. H.; Zhang, Z. D.; Wang, D. S. Low-dimensional material supported single-atom catalysts for electrochemical CO_2 reduction. *SmartMat* **2022**, *3*, 84–110.

[42] Zhang, N. Q.; Zhang, X. X.; Tao, L.; Jiang, P.; Ye, C. L.; Lin, R.; Huang, Z. W.; Li, A.; Pang, D. W.; Yan, H. et al. Silver single-atom catalyst for efficient electrochemical CO_2 reduction synthesized from thermal transformation and surface reconstruction. *Angew. Chem. Int. Ed.* **2021**, *60*, 6170–6176.

[43] Zhang, N. Q.; Zhang, X. X.; Kang, Y. K.; Ye, C. L.; Jin, R.; Yan, H.; Lin, R.; Yang, J. R.; Xu, Q.; Wang, Y. et al. A supported Pd_2 dual-atom site catalyst for efficient electrochemical CO_2 reduction. *Angew. Chem. Int. Ed.* **2021**, *60*, 13388–13393.